Stability of a sloping interface in a rotating two-fluid system

By DESIRAJU B. RAO and T. J. SIMONS, *Department of Atmospheric Science, Colorado State University, Fort Collins, Colo 80521, USA*

(Manuscript received April 9, 1970)

ABSTRACT

When two incompressible homogeneous fluids in relative motion are stratified in a gravitationally stable configuration and are subjected to rotation about a vertical axis, the interface and the free surface slope away from the horizontal. Such a system possesses rotational modes of oscillation in addition to the external and internal gravitational modes. The dynamic stability of small amplitude motions superimposed on this system is studied. For unstable modes, the phase speeds and the growth rates are presented as a function of wavelength of the perturbations and shear of the basic flow. In particular, it is shown that the instability can occur as a result of a coupling between an internal gravitational mode and a rotational mode.

I. Introduction

We are concerned here with the dynamic stability of the equilibrium configuration shown in Fig. 1 with respect to small amplitude perturbations. This configuration consists of two incompressible homogeneous fluids of densities ϱ_1 and ϱ_2 superimposed one on top of another with the heavier fluid (ϱ_1) at the bottom to insure gravitational stability of the system. These fluids are laterally bounded by rigid walls at $y=0$ and $y=W$ and each fluid is moving in the positive x-direction with a constant translational velocity $\bar{u}_1$ and $\bar{u}_2$ ($\bar{u}_1 \neq \bar{u}_2$ in general). In the absence of rotation, the fluids will have uniform depths ($\overline{D}_1$ and $\overline{D}_2$ as shown by the dotted lines in Fig. 1). In this case, the system is only capable of exhibiting gravitational (external and internal) modes of oscillation and any dynamic instability that is realized is purely a manifestation of the Kelvin-Helmholtz instability. As is well known, this instability is usually restricted to rather small wavelengths of the perturbations. If, however, we now assume that the system is rotating about a vertical axis with angular speed Ω, the depths of the fluids can no longer be uniform. The translational velocities $\bar{u}_1$ and $\bar{u}_2$ bring into play the Cariolis forces which would then require balancing pressure gradients. These are generated by the interface and free surface sloping away from the horizontal as shown in Fig. 1. Under these conditions, the system exhibits an additional mode of oscillation—the rotational mode which is normally referred to as the Rossby mode in meteorology—in addition to the gravity modes. The features of these rotational modes normally resemble the characteristics of meteorologically important wave motions that are observed on synoptic weather maps. Our primary concern here is to investigate the stability of the basic state which possesses both the gravitational and rotational modes.

The study of the above stability problem has an application to the problem of frontal instability in meteorology. The Bergen school of Norway has demonstrated that instability associated with narrow transition zones between warm and cold air masses is a possible factor

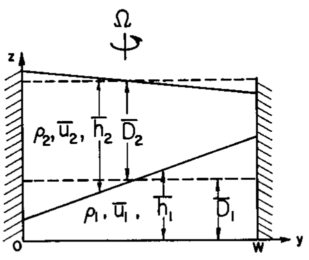

Fig. 1. Equilibrium configuration of the physical model.

in determining the growth of a perturbation in the middle latitudes. In an idealized situation, one can represent each of these air masses by a homogeneous incompressible fluid and the transition zone by a surface of zero-order discontinuity—called the front—with respect to density and tangential velocities. The dominant characteristics of the frontal model are that the frontal surface is inclined at an angle to the horizontal and intersects the ground. One of the earliest attempts at a mathematical analysis of this model is that of Solberg (1928). His model consisted of a rigid top and bottom both of which are inclined at the same angle to the horizontal as the frontal surface. In spite of this simplicity, Solberg's results showed that it is indeed possible to have unstable waves whose wavelengths are approximately in the range of incipient cyclones when the frontal surface is no longer horizontal. It may be recalled that without the sloping front, the only instability the two-fluid system can give is the Kelvin-Helmholtz instability, which is usually confined to wavelengths much smaller than the scale of the incipient cyclones for reasonable values of shear $(\bar{u}_2 - \bar{u}_1)$. Subsequent to Solberg, the mathematical analysis of the frontal problem was done by Kotschin (1932) and Eliasen (1960) with rigid top models in which the frontal surface intersects the ground. Recently Orlanski (1968) made a more elaborate analysis of the Kotschin model.

Most of the traditional stability analyses in meteorology are made for the long planetary waves for which the so-called quasi-geostrophic approximation is introduced. This approximation, first introduced by Charney (1947), effectively filters out the gravity waves leaving only the rotational waves in the system. Use of this approximation greatly simplifies the necessary mathematical analysis. However, when one is concerned with the stability of perturbations of a smaller scale—as those on a frontal surface—this approximation can no longer be justified. Consequently, one has to deal with a non-geostrophic system containing both gravitational and rotational modes. There have been some studies of this ageostrophic stability problem (Arnason, 1963; Derome & Wiin-Nielsen, 1966; Stone, 1966; Sela & Jacobs, 1968) but the precise nature of the stability character and the interaction between the gravitational and rotational modes, if any, is not properly brought out. In the previously mentioned studies on frontal stability, the analysis of the problem was quite complicated in view of the frontal intersection with the ground and the role of the ageostrophic effects introduced by the presence of the gravity waves is not clearly brought out either. It is with a view to investigate this aspect while trying to keep the necessary analysis simple, that we selected the model described earlier. Since the characteristic feature of the frontal theory is the inclination of the front, rather than its intersection with the ground, the results obtained here may still be applicable in an approximate sense to a frontal situation.

II. Dynamical equations

The physical model is described in the preceding section. As mentioned there, we are dealing with motions whose scales are much smaller than the radius of the earth. Consequently, these motions may be described using a Cartesian x, y-plane with a constant Coriolis parameter $f = 2\Omega \sin \phi$, Ω being the angular speed of rotation and ϕ is the geographical latitude. We further assume that the scale of the motions is such that the hydrostatic- or the long wave-approximation is valid. Then the motion in each layer can be described by the shallow water equations:

$$\frac{d\mathfrak{V}_1}{dt} - f[\mathfrak{V}_1] = -g(\varepsilon \nabla h_2 + \nabla h_1) \tag{2.1}$$

$$\frac{dh_1}{dt} + h_1 \nabla \cdot \mathfrak{V}_1 = 0 \tag{2.2}$$

$$\frac{d\mathfrak{V}_2}{dt} - f[\mathfrak{V}_2] = -g(\nabla h_2 + \nabla h_1) \tag{2.3}$$

$$\frac{dh_2}{dt} + h_2 \nabla \cdot \mathfrak{V}_2 = 0 \tag{2.4}$$

In these equations, the subscript 1 refers to the quantities in the lower layer and subscript 2 to those in the upper layer. $\mathfrak{V} = (u, v)$ is the horizontal velocity vector, h is the depth of a layer. The vector $[\mathfrak{V}]$ denotes a rotation of $\mathfrak{V}$ through ninety degrees in the negative sense of the x, y-plane. $\varepsilon \equiv \varrho_2/\varrho_1$ is the density ratio and for a gravitationally stable configuration $0 < \varepsilon < 1$.

The system of equations (2.1) to (2.4) has an exact solution corresponding to the basic state

$$\bar{\mathbf{V}}_1 = (\bar{u}_1, 0) \qquad \bar{\mathbf{V}}_2 = (\bar{u}_2, 0)$$

$$\frac{d\bar{h}_1}{dy} = \bar{\alpha}_1 f \qquad \frac{d\bar{h}_2}{dy} = \bar{\alpha}_2 f \tag{2.5}$$

where we have defined

$$\bar{\alpha}_1 \equiv \frac{\varepsilon\bar{u}_2 - \bar{u}_1}{g(1-\varepsilon)} \qquad \bar{\alpha}_2 \equiv \frac{\bar{u}_1 - \bar{u}_2}{g(1-\varepsilon)} \tag{2.6}$$

We now assume that the translational velocities $\bar{u}_1$ and $\bar{u}_2$ in the basic state are constant $(\bar{u}_1 \neq \bar{u}_2)$ and that the domain of interest is bounded by rigid boundaries at $y=0$ and $y=W$. The depths of the lower and upper fluid layers are then given by (for $y>0$):

$$\bar{h}_1 = \bar{D}_1 + \bar{\alpha}_1 f\left(y - \frac{W}{2}\right)$$

$$\bar{h}_2 = \bar{D}_2 + \bar{\alpha}_2 f\left(y - \frac{W}{2}\right) \tag{2.7}$$

where $\bar{D}_1$ and $\bar{D}_2$ are the layer depths at $y = W/2$. They are also the uniform depths that the fluid layers will have in the absence of rotation.

The dynamical equations (2.1–4) are now linearized about the state of equilibrium expressed through equations (2.5, 2.7) for the examination of the stability problem. The linearized equations are

$$L_j u_j - f v_j + g\left(\frac{\partial h_1}{\partial x} + \gamma_j \frac{\partial h_2}{\partial x}\right) = 0 \tag{2.8}$$

$$L_j v_j + f u_j + g\left(\frac{\partial h_1}{\partial x} + \gamma_j \frac{\partial h_2}{\partial y}\right) = 0 \tag{2.9}$$

$$L_j h_j + \bar{\alpha}_j f v_j + \bar{h}_j\left(\frac{\partial u_j}{\partial x} + \frac{\partial v_j}{\partial y}\right) = 0 \tag{2.10}$$

where $j=1$ or 2 and u_j, v_j, h_j are perturbation quantities.

We have defined

$$\gamma_1 \equiv \varepsilon \quad \text{and} \quad \gamma_2 \equiv 1$$

$$L_j \equiv \frac{\partial}{\partial t} + \bar{u}_j \frac{\partial}{\partial x} \tag{2.11}$$

The equations (2.8–10) represent a coupled set of six homogeneous equations in as many unknowns. The necessary boundary conditions to be adjoined in order to complete the specification of the problem are:

$$u_j, v_j, h_j \text{ are periodic in } x \tag{2.12}$$

and $\quad v_j = 0$ at $y=0$ and W

In the next section we outline the method of solution for the boundary value problem (2.8–12).

III. Method of solution

The coefficients in the dynamical equations (2.7–10) are constants in x so that a solution of the form

$$u_j = U_j(y,t)\,e^{ikx},\ v_j = V_j(y,t)\,e^{ikx}$$

$$j = 1,2. \tag{3.1}$$

$$h_j = H_j(y,t)\,e^{ikx}$$

automatically satisfies the equations and the boundary condition in x. Substitution of this into the equations yields

$$\frac{\partial U_j}{\partial t} + ik\bar{u}_j U_j - f V_j + ikg(H_1 + \gamma_j H_2) = 0 \tag{3.2}$$

$$\frac{\partial V_j}{\partial t} + ik\bar{u}_j V_j + f U_j + g\left(\frac{\partial H_1}{\partial y} + \gamma_j \frac{\partial H_2}{\partial y}\right) = 0 \tag{3.3}$$

$$\frac{\partial H_j}{\partial t} + ik\bar{u}_j H_j + \bar{\alpha}_j f V_j + \bar{h}_j\left(ikU_j + \frac{\partial V_j}{\partial y}\right) = 0 \tag{3.4}$$

with boundary conditions $V_j = 0$ at $y=0$ and W.

This system of equations has been solved by spectral and by finite difference methods. Considering first the spectral solution, we seek solutions of the form

$$V_j(t,y) = \sum_{l=0}^{\infty} V_j^l(t) \sin\frac{l\pi y}{W} \tag{3.6}$$

in order to satisfy the lateral boundary conditions. Since now V_j is an odd function of y, it follows from the equations that U_j and H_j are even functions of y, thus

$$U_j(t,y) = \sum_{l=0}^{\infty} U_j^l(t) \cos \frac{l\pi y}{W} \tag{3.7}$$

$$H_j(t,y) = \sum_{l=0}^{\infty} H_j^l(t) \cos \frac{l\pi y}{W}$$

and further f is an odd function and $\bar{h}_j$ is an even function of y to satisfy the appropriate parities of all quantities in a mathematical sense. Again on a mathematical plane, if all integrations are performed over an interval $-W < y < W$, then sines and cosines are orthogonal and all odd functions integrate out.

Substituting the expansions (3.6, 3.7) into the dynamical equations (3.2, 3.3, 3.4), multiplying the U_j, H_j – equations by $\cos n\pi y/W$ and the V_j – equation by $\sin n\pi y/W$, and integrating over the interval $0 < y < W$, we obtain the spectral equations

$$\frac{dU_j^n}{dt} + ik\bar{u}_j U_j^n - \sum_{l=0}^{\infty} \delta_n f^{ln} V_j^l + ikg(H_1^n + \gamma_j H_2^n) = 0 \tag{3.8}$$

$$\frac{dV_j^n}{dt} + ik\bar{u}_j V_j^n + \sum_{l=0}^{\infty} f^{nl} U_j^l - \frac{n\pi g}{W}(H_1^n + \gamma_j H_2^n) = 0 \tag{3.9}$$

$$\frac{dH_j^n}{dt} + ik\bar{u}_j H_j^n + \sum_{l=0}^{\infty} \delta_n \left[\bar{\alpha}_j f^{ln} V_j^l + \bar{h}_j^{ln} \left(ikU_j^l + \frac{l\pi}{W} V_j^l \right) \right] = 0 \tag{3.10}$$

where $n = 0, 1, 2, \ldots$, $\delta_n = 1$ for $n \neq 0$ and $\delta_n = \frac{1}{2}$ for $n = 0$, and the coefficients are defined as follows:

$$f^{ln} \equiv \frac{2}{W} \int_0^W f \sin \frac{l\pi y}{W} \cos \frac{n\pi y}{W} \, dy$$

$$\bar{h}_j^{ln} = \frac{2}{W} \int_0^W \bar{h}_j \cos \frac{l\pi y}{W} \cos \frac{n\pi y}{W} \, dy \tag{3.11}$$

which can be computed once f and $\bar{h}_j$ have been specified as functions of y.

For computational purposes the series must be truncated, say at $n = N$. We have then a system of $6\,(N+1)$ prediction equations, but since (3.9) can be discarded for $n = 0$, we have only $6N + 4$ coupled equations. The system can be cast into the form

$$\frac{d\mathbf{a}}{dt} + ik\mathcal{A}\,\mathbf{a} = 0 \tag{3.12}$$

where $\mathbf{a}$ is the column vector consisting of the $6N+4$ time-dependent variables and $\mathcal{A}$ is a matrix of order $(6N+4) \times (6N+4)$ with time-independent elements. The solution of (3.12) is of the form

$$\mathbf{a} \sim e^{-ikct} \tag{3.13}$$

Substitution of (3.13) into (3.12) yields the equation:

$$(\mathcal{A} - c\,\mathrm{II})\,\mathbf{a} = 0 \tag{3.14}$$

which shows that the c's are the characteristic values of the matrix $\mathcal{A}$. Combining this time dependent part of the solution with the x-dependent part given by (3.1) we see that the perturbation quantities u_j, v_j, h_j are proportional to $\exp[ik(x - ct)]$. Thus a positive real value for c represents waves progressing in the positive x-direction. If c is complex then a positive imaginary part will give an exponential growth in time for the perturbations, which are then considered unstable. In the present problem complex roots occur in conjugate pairs, thus any growing root is accompanied by a decaying root. However in the Fourier integral representation of an arbitrary disturbance, this decaying wave would not make any significant contribution.

For an independent test of the spectral solution we have also obtained the solutions to the system [3.2] through [3.5] by finite difference methods. The boundary conditions [3.5) suggest the use of a staggered grid system. The channel width W is subdivided into $(N+1)$ strips, the variables U_j and H_j are defined at the centers of the strips, the variables V_j are defined at the boundaries (where they are zero) and between the strips. Derivatives with respect to y are replaced by central differences. Again we obtain a system of $6N+4$ variables which are only time-dependent and the system can be written in the form (3.12).

The stability calculations discussed in the following section have been computed by both methods. The results were essentially the same, but the spectral method showed somewhat better convergence and therefore only the spectral results are presented in the following. Table 1 shows a typical convergence pattern for both methods. The occurrence of the two pairs of

Table 1. *Convergence test for complex eigen values*

Wave speeds c_r and e-folding times $1/kc_i$ as a function of truncation, N. k, wave number; FD, finite difference method; SP, spectral solution. In this table $\bar{u}_1 = 10$ m sec^{-1}, $\bar{u}_2 = 40$ m sec^{-1}, $\varepsilon = 0.98$, $W = 500$ km $\bar{D}_1 = \bar{D}_2 = 5$ km.

	kW = 1		kW = 2	
n	FD c_r $1/kc_i$	SP	FD	SP
1	12.92 ± 2.493 37.09 ± 2.530	14.14 ± 1.878 35.86 ± 1.905	12.86 ± 1.529 37.17 ± 1.526	14.01 ± 1.124 36.02 ± 1.124
3	14.34 ± 2.018 35.69 ± 2.060	14.73 ± 1.928 35.30 ± 1.973	14.33 ± 1.264 35.73 ± 1.260	14.72 ± 1.206 35.35 ± 1.205
5	14.62 ± 1.964 35.41 ± 2.008	14.81 ± 1.927 35.22 ± 1.973	14.63 ± 1.237 35.44 ± 1.233	14.82 ± 1.215 35.25 ± 1.212
7	14.72 ± 1.946 35.31 ± 1.992	14.84 ± 1.926 35.20 ± 1.973	14.73 ± 1.228 35.34 ± 1.225	14.85 ± 1.217 35.23 ± 1.214
9	14.77 ± 1.938 35.26 ± 1.985	14.85 ± 1.926 35.19 ± 1.973	14.78 ± 1.225 35.29 ± 1.221	14.86 ± 1.218 35.21 ± 1.215

complex roots will be explained in the following section.

IV. Results

In determining the characteristic values c of equation (3.14), it is necessary to prescribe the values of the following parameters: $\bar{D}_1$, $\bar{D}_2$, ε, $\bar{u}_1$, $\bar{u}_2$, W, k. In most of the cases, the numerical values assigned to the various parameters are:

$$\bar{u}_1 = 10 \text{ m/sec}$$

$$\varepsilon = 0.98,\ f = 10^{-4} \text{ sec}^{-1}$$

$$W = 500 \text{ km}$$

$$\bar{D}_1 = \bar{D}_2 = 5 \text{ km}$$

Then the values of the wave number k and speed of the upper layer $\bar{u}_2$ were varied while determining the characteristic values c. The numerical values for complex c's are presented in Table 2 for a truncation of the spectral series at $N = 9$ in terms of the phase speed c_r and the e-folding time $1/kc_i$ of the perturbations. This then gives a matrix of the size 58×58 for A. The values of c_r and c_i shown in this table have converged quite well. This can be seen by an examination of Table 1, in which c_r and e-folding time are presented as a function of the size of the matrix A. The bars in Table 2 represent computations which gave stable roots only.

A rather curious feature of the results presented in Table 2 is that when instability occurs, we seem to obtain two pairs of complex roots $c = c_r \pm ic_i$ and $c' = c'_r \pm ic'_i$ and they are located symmetrically about the mean speed $\frac{1}{2}(\bar{u}_1 + \bar{u}_2)$ as far as the phase speeds are concerned. This situation holds for $\bar{u}_2 < 45$ m.sec^{-1}. Then we obtain a small stable region before passing on into another region of instability around $\bar{u}_2 = 47.5$ m.sec^{-1}. Further, the instability seems to be bounded on the long-wave and and short wave-side of the spectrum.

The symmetry of the c_r's of the two pairs of roots with respect to the mean speed—as well as the occurrence of two pairs of complex roots—is rather an accident and is due to the choice $\bar{D}_1 = \bar{D}_2$. If $\bar{D}_1 \neq \bar{D}_2$ this symmetry is no longer realized as will be shown later and one of the two sets of complex roots may sometimes disappear as a consequence. The implications of the existence of two unstable roots when they occur together are important in the considerations of the representation of an arbitrary disturbance. In the conventional stability analysis, the existence of an unstable normal mode implies that any arbitrary disturbance will start growing at a rate essentially determined by this mode. However, if two unstable normal modes are present with approximately the same growth rates, whether an arbitrary disturbance starts to grow initially—and if so, at what rate—depends very much on the phase

Table 2. *Spectral model*, $N = 9$, $W = 500$ km, $\varepsilon = 0.98$, $\bar{D}_1 = \bar{D}_2 = 5$ km, $\bar{u}_1 = 10$ m/sec^{-1}

Values of c_r in m/sec and e-folding time in days (in parentheses) are as a function of $(\bar{u}_2 - \bar{u}_1)$ and wave number

$\bar{u}_2 - \bar{u}_1$	kW = 1	1.2	1.5	2.	3.	4.	6.	12.
37.5		28.8 (±.62)	28.9 (±.53)	28.9 (±.45)	29.0 (±.43)	29.0 (±.75)	44.5 (±1.1)	
36.5			28.4 (±.72)				13.2 (±2.2)	
35.5			27.9 (±3.09)				27.9 (±1.9)	
35.0	—	—	—	—	—	—	10.8 (±2.0) 44.6 (±18.0)	
32.5	35.4 (±1.89) 17.2 (±1.88)	35.4 (±1.67) 17.2 (±1.68)	35.4 (±1.52) 17.2 (±1.56)	35.5 (±1.80) 17.2 (±2.14)	—		—	
30.0	35.2 (±1.97) 14.9 (±1.93)	35.2 (±1.69) 14.8 (±1.65)	35.2 (±1.42) 14.8 (±1.40)	35.2 (±1.22) 14.9 (±1.22)	35.2 (±1.66) 14.9 (±2.21)	—	—	
27.5	34.8 (±4.04) 12.8 (±3.43)	34.8 (±3.28) 12.8 (±2.83)	34.8 (±2.54) 12.8 (±2.24)	34.7 (±1.86) 12.8 (±1.70)	34.7 (±1.38) 12.9 (±1.33)	34.6 (±1.75) 13.0 (±2.44)	—	
25.0	—	—	—	—	10.2 (±35.)	10.7 (±4.00) 34.6 (±6.42)	11.1 (±2.81) 34.1 (±2.62)	—
22.5	—	—	—	—	—		—	
20.	—	—	—	—	—	—		
15.	—		—	—	—	—		
10.	—		—	—	—	—		
1.	—		—	—	—	—		

of these two normal modes relative to one another.

Let us now examine the mechanism that is responsible for producing the instability. Information on the mechanism can be obtained by tracing the change in the value of the roots as $\bar{u}_2$ is increased. As mentioned earlier, there are basically three types of modes in the model. (I) external gravitational modes; (II) internal gravitational modes; (III) rotational modes.

When the secular determinant $\mathcal{A}$ is truncated at a size $M \times M$, we get M roots which can then be assigned into each one of the above categories. Tracing the changes in the values of these roots as the shear is increased—or what is the same, $\bar{u}_2$ is increased—helps us identify the mechanism initiating the instability. To keep matters simple, instead of tracing the changes in all the M roots, we will restrict our attention to only those roots which eventually cause instability when the shear has become sufficiently high. It turns out that these roots are partly rotational and partly gravitational (internal). The nature of these roots can be ascertained by comparison with exact solutions for simple cases. Table 3 shows these potentially unstable roots as a function of $\bar{u}_2$ for a specific wave number kW = 1.5. In this table, we have also included for comparison the quasi-geostrophic rotational modes ($k^2(\bar{u} - c)^2 \ll f^2$ and the internal gravitational modes for $f = 0$ ("filtered solutions"). Henceforth, roots corresponding to filtered models will be identified by a karat (e.g. $\hat{c}$). These results show that each pair of roots is symmetrically located with respect to the mean speed $\bar{U} = \frac{1}{2}(\bar{u}_1 + \bar{u}_2)$. We notice from Table 3 that the c_r's for the rotational modes are in the range $\bar{u}_1 < c_r < \bar{u}_2$ and the c_r's for the gravitational modes are in the range $c_r < \bar{u}_1$ and $c_r < \bar{u}_2$ when the shear is small. As the shear—or $\bar{u}_2$—increases one member of the internal gravitational mode pair approaches one of the members of the rotational mode pair while the other member of the gravitational mode pair approaches the second member of the rotational mode pair. This process is illustrated in Fig. 2. In this Fig. the solid lines labelled $\hat{c}_2 - \bar{u}$ and $\hat{c}_4 - \bar{u}$ show the behaviour of the "filtered" solutions—that is, the pure internal gravity wave solution with $f = 0$ and the quasi-geostrophic rotational wave as a function of $\bar{u}_2$. The other two filtered roots $\hat{c}_1 - \bar{u}$, $\hat{c}_3 - \bar{u}$ are in the lower half of the diagram forming a mirror reflection and consequently are not shown in Fig. 2. When filtering is not used and the rotational and gravitational modes exist together, the behaviour of the roots is shown by the solid

Table 3. *The mechanism of mixed-mode instability*

k, 1.5/500 km; W, 500 km; ε, 0.98; $\bar{D}_1 = \bar{D}_2 = 5$ km; $\bar{u}_1$, 10 m/sec, upper table: $\hat{c}_1$ and $\hat{c}_2$, quasi-geostrophic rotational modes. $\hat{c}_3$ and $\hat{c}_4$, basic internal gravity modes for $f = 0$. Lower table: Basic rotational and internal gravitationalmodes of the spectral solution. e-folding time in days in parentheses. $\bar{U} = \frac{1}{2}(\bar{u}_1 + \bar{u}_2)$

$\bar{u}_2$	$\hat{c}_1 - \bar{U}$	$\hat{c}_3 - \bar{U}$	$\hat{c}_4 - \bar{U}$	$\hat{c}_2 - \bar{U}$
30	− 6.5	−19.8	19.8	6.4
32.5	− 7.3	−19.0	19.0	7.2
35	− 8.1	−18.3	18.3	8.0
37.5	− 8.9	−17.4	17.4	8.8
40	− 9.7	−16.3	16.3	9.6
42.5	−10.5	−15.0	15.0	10.4
43.5	−10.8	−14.4	14.4	10.7
44.5	−11.1	−13.9	13.9	11.0
45	−11.3	−13.6	13.6	11.2
45.5	−11.5	−13.2	13.2	11.4
46.5	−11.8	−12.5	12.5	11.7
47.5	−12.1	−11.8	11.8	12.0

$\bar{u}_2$	$c_1 - \bar{U}$	$c_3 - \bar{U}$	$c_4 - \bar{U}$	$c_2 - \bar{U}$
30	− 6.8	−17.2	17.3	6.7
32.5	− 7.9	−15.4	15.5	7.8
35	− 9.1	−13.6	13.8	8.9
37.5		$-11.0 \pm 1.72i$ (2.24)		$11.0 \pm 1.52i$ (2.54)
40.		$-10.2 \pm 2.76i$ (1.40)		$10.2 \pm 2.72i$ (1.42)
42.5		$-9.1 \pm 2.47i$ (1.56)		$9.1 \pm 2.54i$ (1.52)
43.5		$-8.5 \pm 1.57i$ (2.46)		$8.5 \pm 1.74i$ (2.21)
44.5	− 9.9	− 5.5	5.7	9.8
45.	−10.4	− 3.6	3.8	10.3
45.5	−10.9	$.1 \pm 1.25i$ (3.09)		10.8
46.5	−11.6	$.1 \pm 5.36i$ (.72)		11.5
47.5	−12.2	$.1 \pm 7.33i$ (.53)		12.2

lines labelled $c_2 - \bar{u}$ and $c_4 - \bar{u}$. It is seen that the modified roots c_2 and c_4 come together at a critical value of $\bar{u}_2$ and instability is then initiated. The magnitude of c_i is then given by the vertical distance between the solid and dashed lines. The instability persists until another critical value of $\bar{u}_2$ is reached and represents the primary region of instability shown in Table 2. At the second critical value of $\bar{u}$ the modes separate and we get a stable region. By a comparison with the filtered solutions, we see that for further increase in $\bar{u}_2$ the value of $c - \bar{U}$ decreases for the gravitational mode and increases for the rotational mode. This situation continues until another critical value of $\bar{u}_2$ is reached when the gravitational mode c_4 meets its counter part c_3 coming from below the axis $c - \bar{U} = 0$. At this point, the instability occurring for higher values of $\bar{u}_2$ in Table 2 is obtained. The instability now is generated by gravitational modes alone and hence is of the Kelvin-Helmholtz type modified by effects of rotation. The Kelvin-Helmholtz instability in the presence of rotation occurs for a lower shear (or $\bar{u}_2$) than in the case of $f = 0$, as shown in Fig. 3 where the filtered gravitational modes $\hat{c}_3$, $\hat{c}_4$ come together at a much larger value of $\bar{u}_2$ to generate instability. Thus rotation, in addition to introducing the primary instability region, also seems to increase the Kelvin-Helmholtz instability. In any case, the *primary instability is the result of a coupling between a wave of the internal gravitational type and a wave of the rotational type.* The choice $\bar{D}_1 = \bar{D}_2$ in the present example produces the result that when c_2 and c_4 merge together, so do the roots c_1 and c_3 yielding the second complex mode. When $\bar{D}_1 \neq \bar{D}_2$, one of the two sets of complex modes may be eliminated. This is due to the fact that the c_r's of the gravitational and rotational modes are no longer symmetric with respect to the mean speed and when a confluence of the

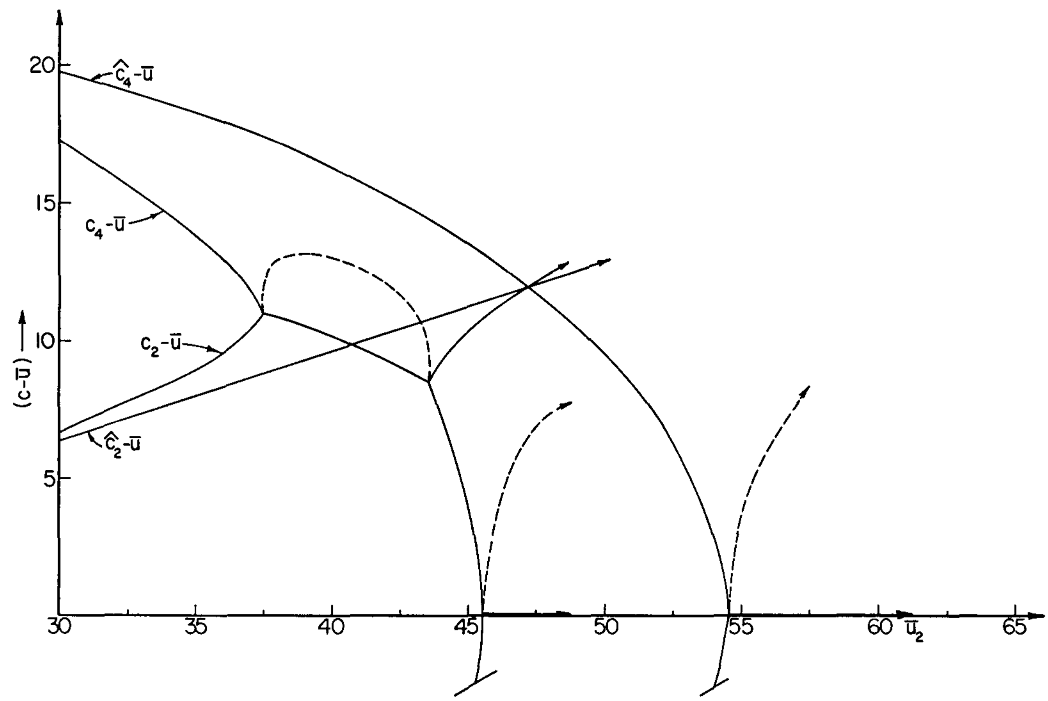

Fig. 2. Illustration of the confluence of gravitational and rotational modes to initiate instability. Curves labelled $\hat{c}_4 - \bar{u}$ and $\hat{c}_2 - \bar{u}$ are the filtered gravitational and rotational modes. The labelled $c_4 - \bar{u}$ and $c_2 - \bar{u}$ curves correspond to the non-filtered situation. The dashed curves represent the imaginary part c_i, whose magnitude is given by the vertical distance between the solid line and the dashed line.

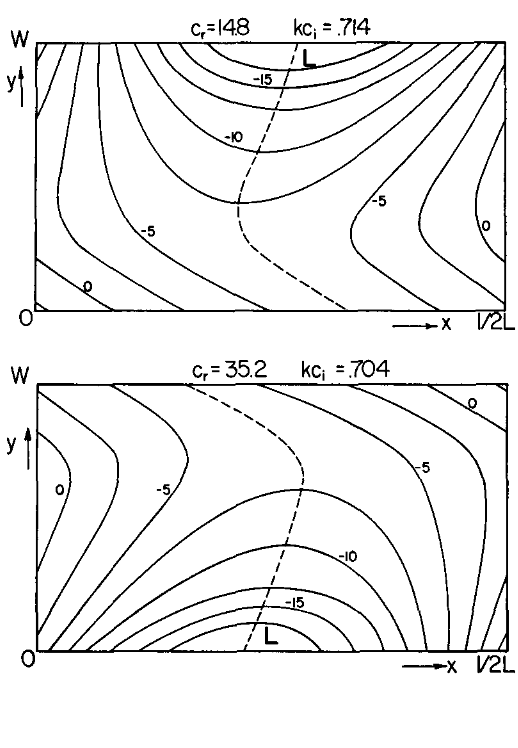

above type occurs between say c_2 and c_4 the other members c_1 and c_3 are still far apart. This will be discussed in more detail in connection with Table 4.

The instability mechanism generated by a coupling between a gravity mode and a rotational mode is a rather unique one. This mechanism straddles the fence—so to say—between the instability mechanisms for the large scale motions and the small scale motion. In the case of the large scale motions, one can study the dynamics of instability in the framework of a filtered system of equations in which the gravity waves are no longer present. Hence the instability, when obtained, must be brought about purely by the rotational modes. On the other hand, earth's rotation is relatively unimportant for small scale motions and their instability, like the Helmholtz instability for example, is purely governed by the spectrum of the gravity modes. For medium scale mo-

Fig. 3. Structures of the two unstable modes in terms of h_1 in the primary instability region.

tions, as the ones considered here, the spectrum of the gravitational and rotational modes are equally important and elimination of either one of these classes of modes might in some cases eliminate any possible instability that the system is capable of exhibiting.

Even though in the model considered so far, the free surface is supposed to represent the tropopause, in reality the atmosphere extends far above the tropopause. To simulate this, we have superimposed a third layer of infinite depth on top of the second layer. In order to keep the slope of the second surface unchanged, the third layer is assumed to have the same constant translational speed as the second layer under equilibrium conditions; that is, $\bar{u}_3 = \bar{u}_2$. The dynamical equations formally look the same as those given by (2.8–10) except for a slight re-definition of the pressure gradient terms and the method of analysis of the preceding section goes through without any modifications. The results for c_r and the growth rate for the case with infinitely deep third layer are shown in Table 4 as a function of $\varepsilon' = \varrho_3/\varrho_2$ for a wave number kW = 1.5 and $\bar{u}_2 = 40$ m/sec. It is seen from this that when ε' is less than about 0.9, there does not appear to be much effect of the third layer on the stability character. However, when $\varepsilon' = 0.98$, one of the two unstable pairs has disappeared and we now have only one unstable normal mode. This mode propagates with a phase speed closer to the speed of the upper layer. The mechanism of instability may be shown to be still the same as before. The presence of the upper layer has a slight tendency to reduce the stability.

Table 4. *Effect of increasing depth of second layer or adding a third layer of infinite depth*

$\bar{u}_3 = \bar{u}_2$, $\varepsilon' \equiv \varrho_3/\varrho_2$. Values of the parameters $k = 1.5/$ 500 km, $W = 500$ km, $\varepsilon = 0.98$, $\bar{u}_1 = 10$ m/sec, $\bar{u}_2 =$ 40 m/sec, $\bar{D}_1 = 5$ km

	$\varepsilon' = 0$			$\bar{D}_2 = 6$	
D_2	c_r	$1/kc_i$	ε'	c_r	$1/kc_i$
5	35.2	± 1.42	0	35.2	± 1.42
	14.8	± 1.40		14.8	± 1.40
6	35.6	± 1.56	.9	35.3	± 1.44
	11.9	± 4.37		16.3	± 1.56
10	36.2	± 2.40	.98	35.5	± 1.58
15	36.5	$\pm 43.$	.99	35.7	± 1.77
20	Stable		1.0	Stable	

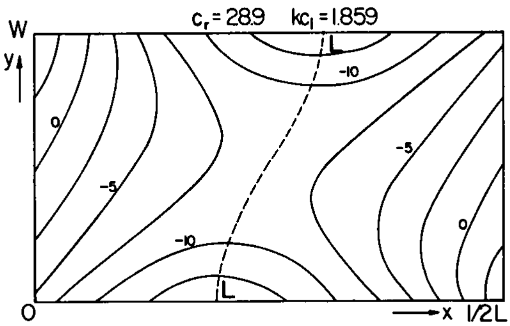

Fig. 4. Structure of the unstable mode in the secondary region of instability.

Continuing with the effects of upper layers on the stability, let us now consider the effect of increasing the depth of the upper layer while keeping the lower layer depth the same as before. The results of this are also given in Table 4. As one might expect, the increase in the depth of the upper layer tends to stabilize the configuration. It may also be noticed that once the uniform depths $\bar{D}_1$ and $\bar{D}_2$ are quite different, one of the unstable modes is eliminated.

We next consider the effect of different depths on the stability. It is found that instability is initiated at a smaller value of the shear $(\bar{u}_2 - \bar{u}_1)$ if $\bar{D}_1$ is small. Further, the region of stability that is obtained in Table 2 for higher values of shear is decreased for $\bar{D}_1 = 4$ km and disappears altogether for $\bar{D}_1 = 3$ km. As before, the presence of a third layer of different density or making $\bar{D}_1/\bar{D}_2/1$, eliminates one of the two unstable pairs.

The structures of the unstable modes are shown in Figs. 3 and 4. The top picture in Fig. 3 corresponds to the mode which is later eliminated by having either a third layer or an unequal $\bar{D}_1$ and $\bar{D}_2$. The bottom picture in Fig. 3 shows the height distribution for the mode with its phase speed closer to the upper layer speed. It shows that development takes place closer to the $y = 0$ boundary or the low levels. Fig. 4 shows the structure of the unstable normal mode at $\bar{u}_2 = 47.5$ m/sec^{-1}.

V. Summary and Conclusions

The problem of non-geostrophic instability of a two-fluid system in a channel has been considered. It was shown that the primary instability in this model is realised as a result of an interaction between a gravitational and rotational mode. As the channel width is increased, the mixed mode instability maybe shown to be gradually replaced by quasi-geostrophic instabilities (Rao & Simons, 1969). In another study, Simons & Rao (1970), considered a two-layer model without lateral boundaries so that an exact analytical solution could be obtained under the approximation that the layer depths are treated as constant except when differentiated. That study shows that the mixed mode instability occurs as a patch in a region where neither the Helmholtz type instability nor the quasi-geostrophic instability exists.

The mixed mode instability obtained in this problem is, of course, completely dependent on the non-geostrophic nature of the problem. The question of interest now is whether the mechanism of instability obtained in this work is typical of more non-geostrophic situations. The non-geostrophic stability studies of a continuous atmosphere by Arnason (1963), and Derome & Wiin-Nielsen (1968) show that their instability is primarily of the geostrophic type. However, numerical experiments on the same model conducted by discretising the vertical dependency by finite-difference levels indicated the possibility of obtaining a mixed type of instability in regions where the geostrophic instability is either absent or very weak. The appearance of this mixed instability is rather inconsistent in the sense that an unstable mode at a certain resolution in the vertical seems to be replaced by a different unstable mode at a different resolution. In any case, it appears certain that the mixed instability is present in a system in which the continuous vertical nature of the atmosphere is replaced by a finite number of levels. Consequently, one may consider the possibility that this instability is a mathematically introduced phenomenon, in which case it may lead to considerable difficulties in any numerical model of a non-geostrophic atmosphere.

As far as the physical relevance of such an instability mechanism is concerned, it should be remembered that the model considered here is set up as an approximation to a frontal situation. Since a frontal phenomenon is somewhat of a discontinuous nature, it is quite plausible that a mechanism of the type described here may be operative in generating the instability.

Acknowledgements

We are grateful to Dr Akira Kasahara of the National Center for Atmospheric Research, Boulder, for several helpful discussions and to Dr Ferd Baer for a review of the manuscript. Part of this work was done while one of the writers (DBR) was at NCAR, Boulder and the Marine Sciences Branch, Dept. of Energy, Mines and Resources, Ottawa. We are grateful to Mrs Sylvia Hargreaves of NCAR and Mr John Taylor of MSB for their help with programming. This research was supported by NSF Grant GA-11637 and Air Force Cambridge Research Labs Contract F 19628-68-C-0104.

REFERENCES

Arnson, G. 1963. The stability of nongeostrophic perturbations in a baroclinic zonal flow. *Tellus 15*, 205–229.

Charney, J. G. 1947. The dynamics of long waves in a baroclinic Westerly current *J. Met. 4*, 135–162.

Derome, J. F. & Wiin-Nielsen, A. 1966. *On the baroclinic stability of zonal flow in simple model atmospheres*. Technical Report. College of Engineering, Univ. of Michigan, Ann Arbor, Mich. 93 pp.

Eady, E. 1949. Long waves and cyclone waves. *Tellus 1*, 33–52.

Kotschin, N. 1932. Über die Stabilität von Margulesschen Diskontinuitäts Flächen. *Beitr. Phys. frei Atmos. 18*, 129–164.

Orlanski, I. 1968. Instability of frontal waves. *J. Atmos. Sci. 25*, 178–200.

Phillips, N. A. 1964. An overlooked aspect of the baroclinic stability problem. *Tellus 16*, 268–270.

Rao, Desiraju B. & Simons, T. J. 1969. *Stability of a sloping interface in a rotating two-fluid system*. Atmospheric Science Paper No. 151, Colorado State Univ., Fort Collins, Colo. 32 pp.

Sela, J. & Jacobs, S. J. 1968. *On baroclinic and barotropic ageostrophic stability*. Technical Report. College of Engineering, Univ. of Michigan, Ann Arbor, Mich. 98 pp.

Simons, T. J. & Rao, D. B. 1970. Instability of rotational and gravitational modes of oscillation. Atmospheric Science Paper No. 155, Colorado State Univ., Fort Collins, Colo. 21 pp.

Solberg, H. 1927. Integrationen der atmosphärischen Störungsgleichungen. *Geofys. Publ. 5*, No. 9, 210 pp.

Stone, P. 1966. On non-geostrophic baroclinic stability. *J. Atmos. Sci. 23*, 390–400.

УСТОЙЧИВОСТЬ НАКЛОННОЙ ПОВЕРХНОСТИ РАЗДЕЛА ВО ВРАЩАЮЩЕЙСЯ ДВУСЛОЙНОЙ ЖИДКОСТИ

Если две несжимаемые однородные жидкости, находящиеся в относительном движении, устойчиво стратифицированы и вращаются вокруг вертикальной оси, то поверхность раздела и свободная поверхность могут отклоняться от горизонтали. Такая система обладает вращательными типами колебаний в добавление к внешним и внутренним гравитационным колебаниям. Изучается динамическая устойчивость малых колебаний такой системы. Для неустойчивых колебаний фазовая скорость и интенсивность роста являются функциями длины волны и сдвига основного потока. В частности показано, что неустойчивость может быть результатом взаимодействия внутренних гравитационных и вращательных колебаний.